Article

Comparative Water Environment Simulation Study of Two Typical Models with BMPs in a Karst Basin

Jing Zhang [1,2,*], Peiqi Zhang [1,2] and Yongyu Song [1,2]

[1]   Beijing Key Laboratory of Resource Environment and Geographic Information System, College of Resource Environment and Tourism, Capital Normal University, Beijing 100048, China; 2200902205@cnu.edu.cn (P.Z.); 2190901014@cun.edu.cn (Y.S.)
[2]   Beijing Laboratory of Water Resources Security, Beijing 100048, China
*   Correspondence: 5607@cnu.edu.cn

Abstract: Carbonate rocks are widely distributed in southwest China, forming a unique karst landscape. The Lijiang River Basin provides a typical example of an area with concentrated karst. Research on the laws of hydrology and water quality migration in the Lijiang River Basin is important for the management of the water resources of Guilin City and similar areas. In this study, we combined three meteorological data with the soil and water assessment tool (SWAT) model and the hydrological simulation program-Fortran (HSPF) model to simulate the hydrological and water quality processes in the Lijiang River Basin separately. We chose the Nash–Sutcliffe efficiency (NSE) coefficient, coefficient of determination (R^2), root mean square error-observations standard deviation ratio (RSR), and mean absolute error (MAE) as the metrics used to evaluate the models. The results, combined with the time-series process lines, indicated that the SWAT model provides a more accurate performance than the HSPF model in streamflow, ammonia nitrogen (NH_3-N), and dissolved oxygen (DO) simulations. In addition, we divided the karst and non-karst areas, and we analyzed the differences between them in water balance, sediment transport, and pollution load. We further identified the key source areas of pollution load in the Lijiang River Basin, evaluated the pollution reduction effect of best management practices (BMPs) on surface source pollution, and proposed some pollution control countermeasures. Each scenario, especially returning farmland to forest and creating vegetation buffer zones, reduces the NH_3-N and DO pollution load.

Keywords: karst area; precipitation; SWAT model; HSPF model; water quality; best management practices

1. Introduction

The landscape in Guilin, China, is mainly composed of the Lijiang River system, and has become a world-famous tourist attraction because of its remarkable karst landforms [1]. The Lijiang River Basin is a developed water system with abundant runoff. In addition, its widely distributed carbonate rocks have had strong karst development under long-term weathering and erosion due to water flow. The karst landforms are striking. The surface of the karst has formed stone buds, dry valleys, and karst ditches while underground, karst caves, shafts, and funnels have been formed [2,3]. These unique karst structures create differences in the spatial structures of the aquifer, and the surface groundwater hydrological cycle of the karst is heterogeneous. Given this natural background, irresponsible human activities in the area have led to vegetation damage, rocky land desertification, exposed bedrock and soil erosion, and the natural ecology is fragile [4–6]. According to the geological conditions of the Lijiang River Basin, a hydrological model of the karst area must be established to study the mechanism of hydrological water quality circulation, to provide a basis for the scientific management of water resources and to protect the ecological uniqueness of the Lijiang River Basin.

Due to the complexity of the watershed physical mechanism, the internal specific hydrological cycle process is difficult to be expressed by a simple formula. The hydrological model can use mathematical methods to abstract and generalize the complex water cycle process, so as to accurately describe and analyze the runoff and confluence process, as well as the water balance of the basin [7]. At present, the hydrological model has shown very strong capabilities in solving many problems such as water resources management, flood control, disaster reduction, and non-point source pollution [8–10].

The soil and water assessment tool (SWAT) model [11], one of the best-known semi-distributed hydrological models, is based on physical mechanisms and it portrays some processes empirically to simulate the hydrological and material cycle at the basin scale [12,13]. For karst landscapes with complex subsurface conditions and special hydrogeological conditions, the SWAT model's simple approach makes it useful in some cases, but it does not consider the special geological formations in karst areas [14,15]. In addition, the hydraulic simulation program-Fortran (HSPF) model, a typical semi-distributed hydrological model, has also been applied in karst areas [16,17]; however, studies of the SWAT and HSPF models are relatively lacking in karst areas within the Chinese region, especially in terms of pollutant simulation, so the applicability of the models in these areas needs to be further validated.

To operate a hydrological model, meteorological data need to be input, one of the most important of which are precipitation data [18,19]. The accuracy of precipitation data seriously affects the results of model simulations and the current precipitation data are mainly obtained from ground station observations, satellite observations, and reanalysis of precipitation. Due to the influence of various factors, the data from surface rainfall observation stations are often unevenly distributed, and in remote mountains and areas with complex terrain, the observation stations are sparse, which leads to a lack of data and difficulties in subsequent observation and maintenance [20]. Therefore, further reanalysis of precipitation data and satellite observation data is particularly important.

The China Meteorological Assimilation Driving Datasets (CMADS) for the SWAT model contain atmospheric assimilation meteorological data jointly researched and developed by Meng et al. [21]. The CMADS series data were sourced from the meteorological observations of more than 30,000 ground observation stations in China and are used for fusion calibration, which improves the availability and accuracy of the CMADS data sets in China [22]. This high-resolution and high-quality data set covers the whole of East Asia [23], and helps to reduce the uncertainty caused by meteorological elements' input; the data set has been the focus of and promoted by many researchers at home and abroad in recent years [24]. The Global Precipitation Measurement (GPM) mission [25] is a remote sensing satellite precipitation data product developed by NASA based on the Tropical Rainfall Measurement Mission (TRMM) [26]. The integrated multi-satellite retrievals for GPM (IMERG) data are the most widely used data in the GPM product series. Compared to TRMM precipitation data, IMERG precipitation data has higher accuracy and wider coverage, including in South China [20,27].

Agricultural non-point pollution is one of the main sources of water pollution in the Lijiang River Basin, and it seriously affects the ecological water environment. Because of the unique karst landform in the Lijiang River Basin, soil erosion occurs frequently and water pollution is aggravated. Therefore, it is essential to prevent and control the non-point-source pollution in the Lijiang River Basin and implement scientific and reasonable management measures. The best management practices (BMPs) are a series of engineering and non-engineering measures widely used to control agricultural non-point-source pollution [28,29]. To achieve water quality goals, management measures can be screened and evaluated using a hydrological model in advance. The SWAT model contains rich agricultural management data. By modifying some parameters or directly adding agricultural measures, the model can easily simulate the changes in non-point-source pollution, to help formulate the BMPs for the treatment of non-point-source pollution [30,31].

At present, although hydrological models are widely used, the accuracy and applicability of various precipitation data are being gradually improved; however, the research on hydrological models and multi-source precipitation data in the Lijiang River Basin with karst landscape is still insufficient. In addition, in order to implement the "Beautiful China" development strategy, it is very necessary to prevent and control non-point-source pollution in the Lijiang River Basin. Taking the Lijiang River Basin as the study area, this paper has the main following objectives: (1) compare and evaluate the applicability of SWAT and HSFP models driven by ground observation precipitation data, CMADS and IMERG, respectively, in the hydrological and water quality simulation of the Lijiang River Basin; and (2) discuss six BMPs scenarios for non-point-source pollution prevention and control based on the simulated results and the karst geological characteristics of the Lijiang River Basin.

2. Materials and Methods

2.1. Study Area

The Lijiang River, located in the northeast of the Guangxi Zhuang Autonomous Region, belongs to the Guijiang River system of the Pearl River Basin (see Figure 1). Originating from the Bajiaotian Alpine swamp zone of the Maoer Mountain in the northwest of Xing'an County, Guilin City, it flows from north to south, with a total length of 214 km and a drainage area of about 5444 km^2 [32]. The Lijiang River Basin has a subtropical monsoon climate with abundant rainfall and high temperatures: the annual average precipitation can reach 1627 mm and the annual average temperature is 19.1 °C. In addition, the region has an annual average sunshine duration of 1553.09 h, frost-free period of 308 days, and an annual average relative humidity of 80%. The area is suitable for the growth and reproduction of animals and plants.
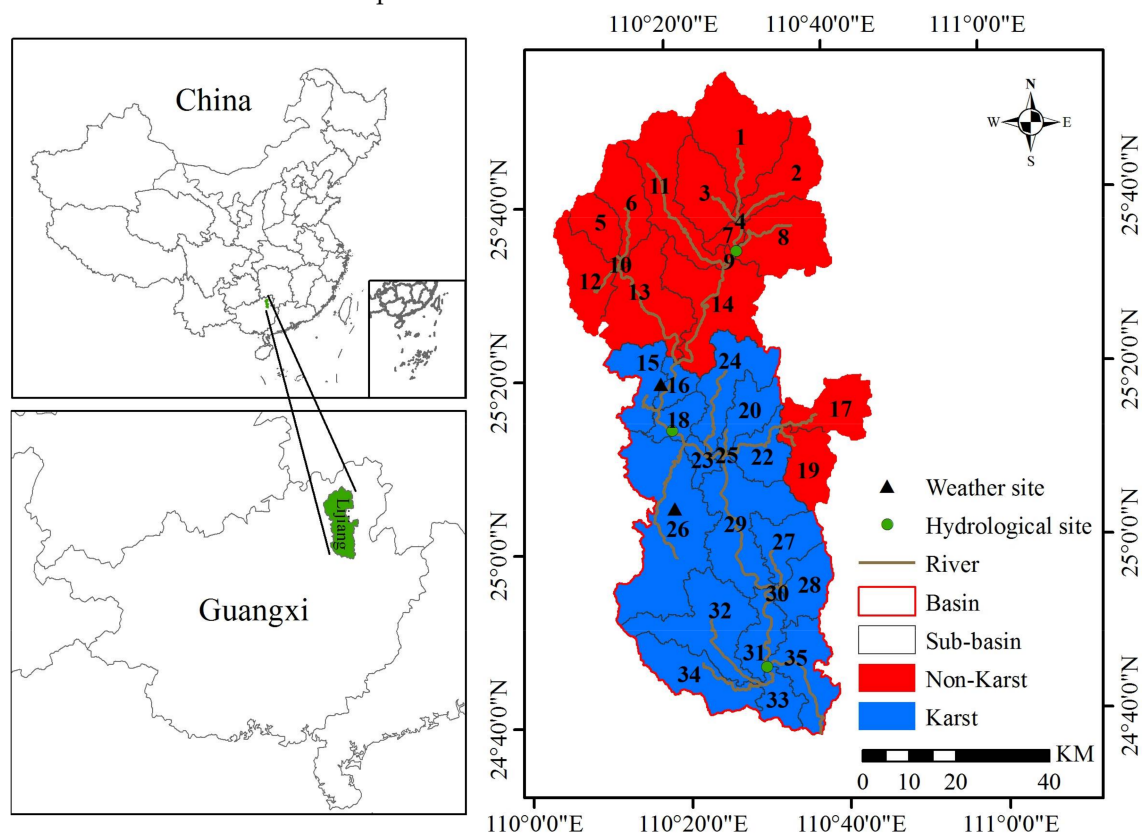

Figure 1. Location of the study area and distribution of sub-basins, karst and non-karst areas.

The Lijiang River is a rain-sourced river. The precipitation in the basin is affected by monsoon activity, and the spatial and temporal distribution of precipitation is unbalanced.

Due to the decrease in the precipitation from north to south and the regular change in the geological characteristics from upstream to downstream in the Lijiang River Basin, the density of the river network is characterized by top-down piecewise runoff. Affected by rainfall, the amount of water in the basin suddenly increases and decreases, which directly affects the water available for industrial supply, agricultural production, and domestic use [33].

The terrain in the Lijiang River Basin is higher in the north and lower in the south, and the river trunk is lower in the middle and higher on both sides. Most of the middle and lower reaches are covered by carbonate, which forms unique karst landforms. The upper reaches can be classified as non-karst areas [34], with geomorphic forms mainly including tectonic erosion and tectonic denudation geomorphology. The middle and lower reaches of the basin can be classified as karst areas, with geomorphic forms mainly including structure dissolution, erosion dissolution, denudation dissolution, sedimentation dissolution, and dissolution accumulation geomorphologies.

2.2. Data Collection

The construction of the SWAT and HSPF models requires the input of spatial geographic data (DEM, land use type, and soil type) and meteorological data (precipitation, evaporation, temperature, runoff, etc.). Spatial geographic data are used to generate rivers, build river networks, divide sub-basins, and generate hydrological response units. The inputs and outputs of the watershed are described by establishing a database based on meteorological data. To calibrate and verify the model, the measured hydrology and water quality data (runoff, sediment, ammonia nitrogen, etc.) are also needed. The sources of the model data are listed in Table 1.

Table 1. Data sources used in this study.

Data	Resolution	Period	Source
DEM	90 m	/	Geospatial data cloud
Land use	300 m	/	Global land cover products of Tsinghua University
Soil	1 km	/	World Soil Database, HWSD
Meteorology	/	2005–2016	China Meteorological Data Network, CMADS, IMERG
Runoff	/	2006–2016	Hydrological yearbook of Pearl River Basin
Sediment	/	2006–2016	Hydrological yearbook of Pearl River Basin
Water quality	/	2008–2016	Environmental Monitoring of China

In this study, we selected three kinds of precipitation data: ground observation data (China surface climate data V3.0 (CSCDS)), CMADS atmospheric assimilation data, and IMERG satellite remote sensing precipitation data. Each data set has a different spatial resolution and starting observation year; the distribution of the number of stations in the Lijiang River Basin also differs. The distribution of CSCDS data is particularly uneven, with only two sites within the Lijiang River Basin, as shown in Figure 1. The spatial resolution of CMADS is 1/3°. We selected a total of eight grids within and around the Lijiang River Basin as the input to the model in this study. IMERG's spatial resolution is 0.25°, and precipitation data were extracted from a total of 104 grids.

As the collection of runoff and CSCDS data was limited to the time periods of 2006–2016 and 2005–2016, respectively, we selected 2005 as the warm-up period for the model in this study, and the data from 2006 to 2016 were used for the calibration and validation of the SWAT and HSPF models. The HSPF model needs evapotranspiration data to operate—although the CMADS and IMERG lack evapotranspiration data, CSCDS does not— therefore we used the CSCDS to drive the two models at the same time. Consequently, the meteorological data except for precipitation are all based on CSCDS data, which facilitates a comparison of the impact of precipitation data on the simulation efficiency of the model.

Before using the three kinds of data to drive the hydrological model, we performed a comparative analysis of their daily precipitation data using the mean average error (MAE) and root mean square error (RMSE). We extracted CMADS and IMERG precipitation data at the CSDCS station locations and averaged them for a more accurate comparison. The analysis showed that the variation in the interannual precipitation trends of the CSCDS, CMADS, and IMERG data were basically the same. Compared with the daily precipitation of the CSCDS data, the MAE values of CMADS and IMERG data were 0.33 mm (7.04%) and 0.43 mm (9.13%), respectively; the RMSE values of CMADS and IMERG data were 8.28 mm and 11.19 mm, respectively. The error between the two kinds of precipitation data and the ground observation station data was small, which was controlled within 10%, indicating that the data quality was reliable; however, the precipitation values of CMADS and IMERG were slightly higher than those of the CSCDS. The calculation formulas of the RMSE and MAE are as follows:

$$MAE = \frac{1}{n}\sum_{i=1}^{n} |O_i - S_i| \tag{1}$$

$$RMSE = \sqrt{\frac{1}{n}\sum_{i=1}^{n} (O_i - S_i)^2} \tag{2}$$

where O_i is the measured runoff value (m^3/s); and S_i is the simulated runoff value (m^3/s).

2.3. Model Setup

We used the ArcGIS platform to analyze and process the DEM, generate the river network and basin boundary, divide the sub-basins, and generate the hydrological response units (HRUs). Simultaneously, we reclassified the land use types, soil types, and slopes. Finally, the whole Lijiang River Basin was divided into 35 sub-basins and 370 HRUs in the SWAT model. These preprocessed data were input into the SWAT and HSPF models for overlay analysis. Finally, we imported the meteorological data to establish engineering files. As the precipitation data were obtained from CSCDS, CMADS and IMERG, the other input elements were kept unchanged, only the precipitation input was changed, and three SWAT engineering files and three HSPF engineering files were created.

Based on the geological characteristics of carbonates and clastic rocks, we divided all sub-basins into two categories: karst areas (carbonates rocks) and non-karst areas (clastic rocks) [35]. The karst-area sub-basins include grids 15, 16, 18, 20–35, covering an area of 2755 km^2; the non-karst sub-basins include grids 1–14, 17, 19, covering an area of 2689 km^2, as shown in Figure 1. After calibration of the SWAT model, the simulation of each hydrological element could be easily consulted in the output file, and the water balance of the basin could be further analyzed. Water balance occurs when the difference between the inputs and outputs of a certain water body (or region) in a certain period are equal to the storage variable of the water body (or region) [36]. The water balance formula of the SWAT model is shown in Equation (3) [35]:

$$\Delta Sw = PREC - SURQ - LATQ - PERC - ET \tag{3}$$

where $\triangle S_W$ is the change in the water storage in the basin (mm); PREC is the rainfall in the basin (mm); SURQ is the surface runoff in the basin (mm); LATQ is the lateral runoff (mm); PERC is the recharge of soil to groundwater (mm); and ET is the actual evapotranspiration (mm).

According to the measured runoff data period, we selected the period from 2006 to 2011 as the calibration period, and the period from 2012 to 2016 as the verification period. We used SWAT Calibration and Uncertainty Programs (SWAT-CUP) software to adjust the parameters of the SWAT model, and we used the Parameter Estimation (PEST) program to adjust parameters of the HSPF model. The selected model hydrological parameters are shown in Table 2.

Table 2. Descriptions of parameters used in the SWAT and HSPF models.

Model	Parameter	Description
SWAT	CN2	Runoff curve number
	ALPHA_BF	Base flow regression coefficient
	GW_DELAY	Groundwater delay time
	GWQMN	The threshold depth at which shallow aquifers produce "base flow"
	RCHRG_DP	Seepage coefficient of deep aquifers
	OV_N	Overland flow Manning coefficient
	SOL_Z	Depth of soil surface to bottom
	CH_K2	Effective hydraulic conductivity of the main riverbed
	REVAPMN	Re-evaporation water level threshold
	ESCO	Soil evaporation compensation coefficient
HSPF	LZSN	Rated accumulation of lower soil layer
	UZSN	Rated accumulation of lower soil layer
	INFILT	Infiltration coefficient
	KVARY	Influencing factor of groundwater subsidence coefficient
	AGWRC	Groundwater regression coefficient
	INTFW	Outflow coefficient in soil
	IRC	Soil flow regression coefficient
	BASETP	Percentage of base flow evapotranspiration
	DEEPER	Proportion of underground outflow into deep groundwater
	SLSUR	Average slope of overflow over slope

2.4. Scenario Setting of BMPs

BMPs are used to control pollution by changing environmental conditions in the basin through engineering and non-engineering measures. Engineering measures are mainly used for pollution reduction, sand reduction, flood control, and other measures with certain physical structures, such as sedimentation ponds, filter strips, wetland buffers, vegetation hedges, etc. Non-engineering measures are the operational procedures for new management measures or improvements to existing management measures, such as tillage management, nutrient management, landscape management, etc. In the SWAT model, the implementation of BMPs can be simulated by changing the values of one or more specific parameters in the .mgt and .ops files in the "subbasins data" module. By artificially setting some scenarios to change the pollutant load, we evaluated the most effective single or comprehensive measures to reduce the pollution load and identified solutions for the prevention and control of water pollution.

Based on the actual agricultural fertilization, planting patterns, and land use in the Lijiang River Basin, we simulated and evaluated six kinds of BMPs, including non-engineering, engineering, and landscape measures. In the initial scenario (scenario 0), no measures were applied, non-engineering measures were implemented in scenarios 1–2, engineering measures were implemented in scenarios 3–5, and landscape measures were considered in scenario 6. Table 3 describes the specific scenario settings.

Table 3. Scenario settings of best management practices.

BMPs	Scenario	Description of Measures	Parameter Adjustment
Initial	0	None	None
Nonengineering measures	1	No tillage	Add tillage to .mgt
	2	Stubble mulching	Add Harvest Only to .mgt
Engineering measures	3	Vegetation buffer zone 10 m	FS is set to 10 in .ops
	4	Grass-planted waterways	Add grassed waterway in .ops
	5	Contour hedgerow	Set FILTERW to 1 in .mgt
Landscape measures	6	Returning farmland to forest (>25°)	Classify cultivated land with a slope above 25° as forest land

2.5. Evaluating Indicators

The goodness of fit index is used to evaluate the degree of fit between simulated and measured values. The commonly used evaluation indexes are the Nash–Sutcliffe efficiency (NSE) coefficient and coefficient of determination (R^2). A SWAT model simulation is generally considered satisfactory when the NSE coefficient and R^2 are greater than 0.5, and the closer their values to 1, the better the simulation effect [37,38]. We also adopted this criterion in this study for the evaluation of the HSPF simulation results. In addition, we used the MAE and RMSE-observations standard deviation ratio (RSR) [39]. The optimal value of RSR is 0. An RSR less than 0.5 indicates that the model performs very well. Lower RSR values indicate a lower root mean square error normalized to the standard deviation of the observations, indicating the accuracy of the model simulation. The NSE, R^2, and RSR calculation formulas are, respectively, as follows:

$$\text{NSE} = 1 - \frac{\sum_{i=1}^{n} (O_i - S_i)^2}{\sum_{i=1}^{n} (O_i - \overline{O})^2} \tag{4}$$

$$R^2 = \frac{\left[\sum_{i=1}^{n} (O_i - \overline{O})(S_i - \overline{S})\right]^2}{\sum_{i=1}^{n} (O_i - \overline{O})^2 \sum_{i=1}^{n} (S_i - \overline{S})^2} \tag{5}$$

$$\text{RSR} = \frac{\sqrt{\sum_{i=1}^{n}(O_i - S_i)^2}}{\sqrt{\sum_{i=1}^{n}(O_i - \overline{O})^2}} \tag{6}$$

where O_i is the measured runoff value (m^3/s); S_i is the simulated runoff value (m^3/s); $\overline{O}$ is the average value of measured runoff (m^3/s); $\overline{S}$ is the average value of simulated runoff (m^3/s); and n is the total number of observation series.

In the evaluation of the simulated management measures, we used the pollution load reduction efficiency as the evaluation index to evaluate the control effect of seven kinds of BMPs on surface source pollution. Reduction efficiency is defined as the ratio of the reduction in pollution load relative to the initial scenario and the pollution load under the initial scenario [40]. The reduction efficiency calculation formula is:

$$R = \frac{\text{Pre}_{BMPs} - \text{Aft}_{BMPs}}{\text{Pre}_{BMPs}} \times 100\% \tag{7}$$

where R is the reduction efficiency (%); Pre_{BMPs} is the pollution load intensity (t/km^2) under the initial scenario; and Aft_{BMP} is the pollution load intensity (t/km^2) after implementing BMP measures.

3. Results and Discussion

3.1. Flow Comparison

The SWAT and HSPF models were driven by CSCDS, CMADS, and IMERG precipitation data to simulate daily runoff. The simulation results are shown in Figures 2 and 3. Table 4 compares the simulation results of the two models driven by the three types of precipitation data.

Both the SWAT and HSPF models obtained satisfactory results for runoff simulations driven by CSCDS precipitation data, with NSE and R^2 above 0.7 for both the calibration and validation periods. The HSPF model was more accurate for some peak flows, whereas the SWAT model simulations better fit the baseflow processes. Driven by CMADS precipitation data, the evaluation indices of both hydrological models were slightly higher than that of CSCDS, with NSE and R^2 above 0.75, and the errors of the simulation results were smaller. Like the CSCDS data-driven models, the HSPF model fit slightly better than the SWAT model at high flow levels during the calibration period, whereas the SWAT model fit better than the HSPF model overall during the validation period. Driven by the IMERG

precipitation data, both models performed somewhat worse than when the other two data sets were input, with the NSE and R^2 above 0.65, while the errors in the simulation results were larger.
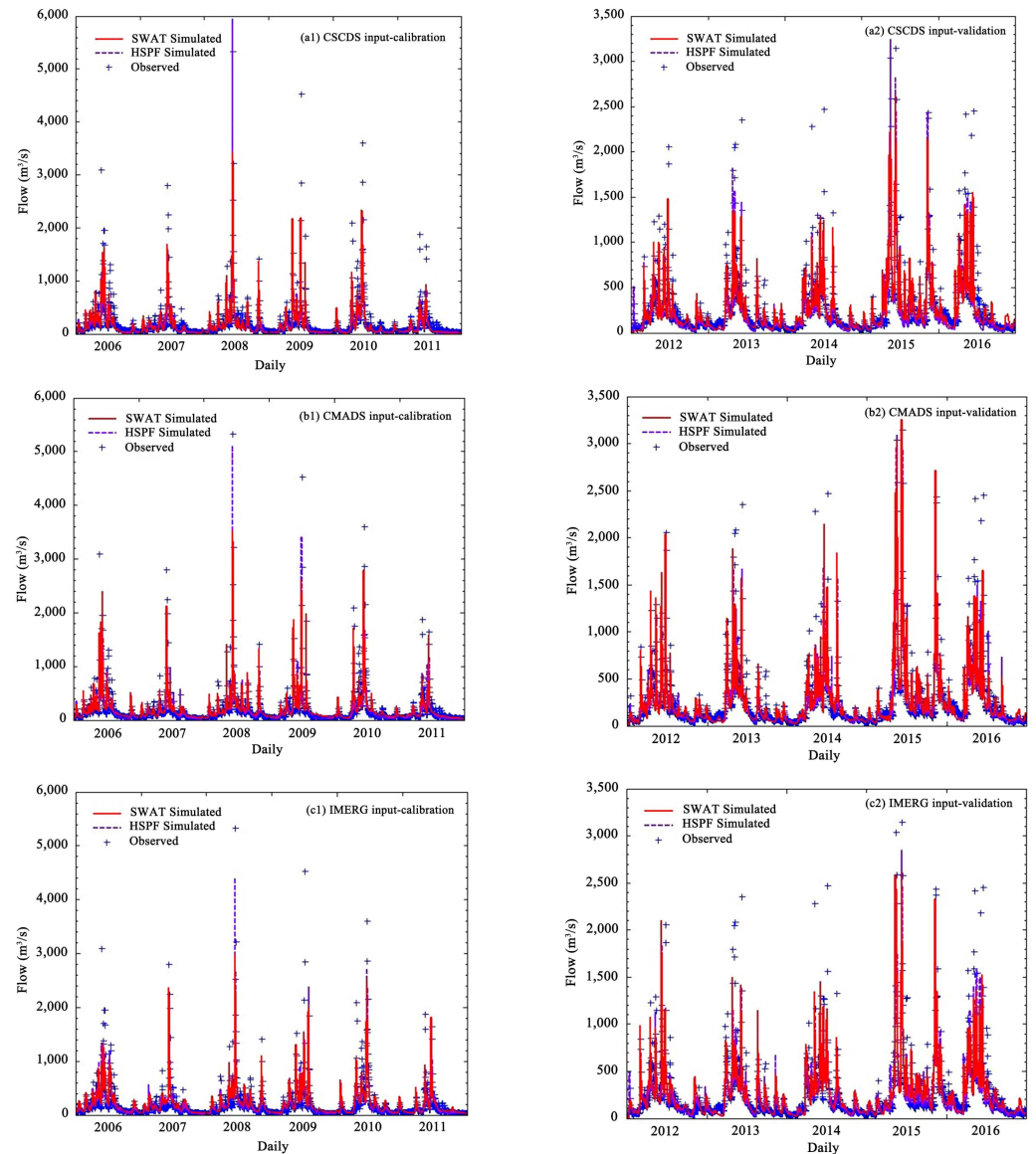

Figure 2. Comparison of the flow hydrograph results produced with the SWAT and HSPF model with (**a1**,**a2**) CSCDS, (**b1**,**b2**) CMADS, and (**c1**,**c2**) IMERG inputs.

Overall, all three data-driven SWAT and HSPF models met the runoff simulation requirements of the Lijiang River Basin, but as precipitation is the most important cause of runoff, the runoff results of the models differed due to the differences in the precipitation data. For the same model, the CMADS data produced a more accurate simulation effect than CSCDS and IMERG data. For the same precipitation data, the SWAT model was more accurate than the HSPF model. We found that the best combination was using CMADS precipitation data to drive the SWAT model, which produced the most accurate simulation effect; however, in some special cases, such as the peak part of the validation period, when driven by IMERG precipitation data, the simulation results of the HSPF model were more accurate than those of the SWAT model. The main reason for this may be that the measured runoff was small, and the average precipitation value in the IMERG data in this period was less than those of CMADS and CSCDS, therefore the runoff value generated by the IMERG-driven model was also small, resulting in a higher consistency with the measured

value. When driven by CMADS precipitation data, the runoff simulation effect of the model was the most accurate. This conclusion laid a foundation for the water quality simulation that followed.
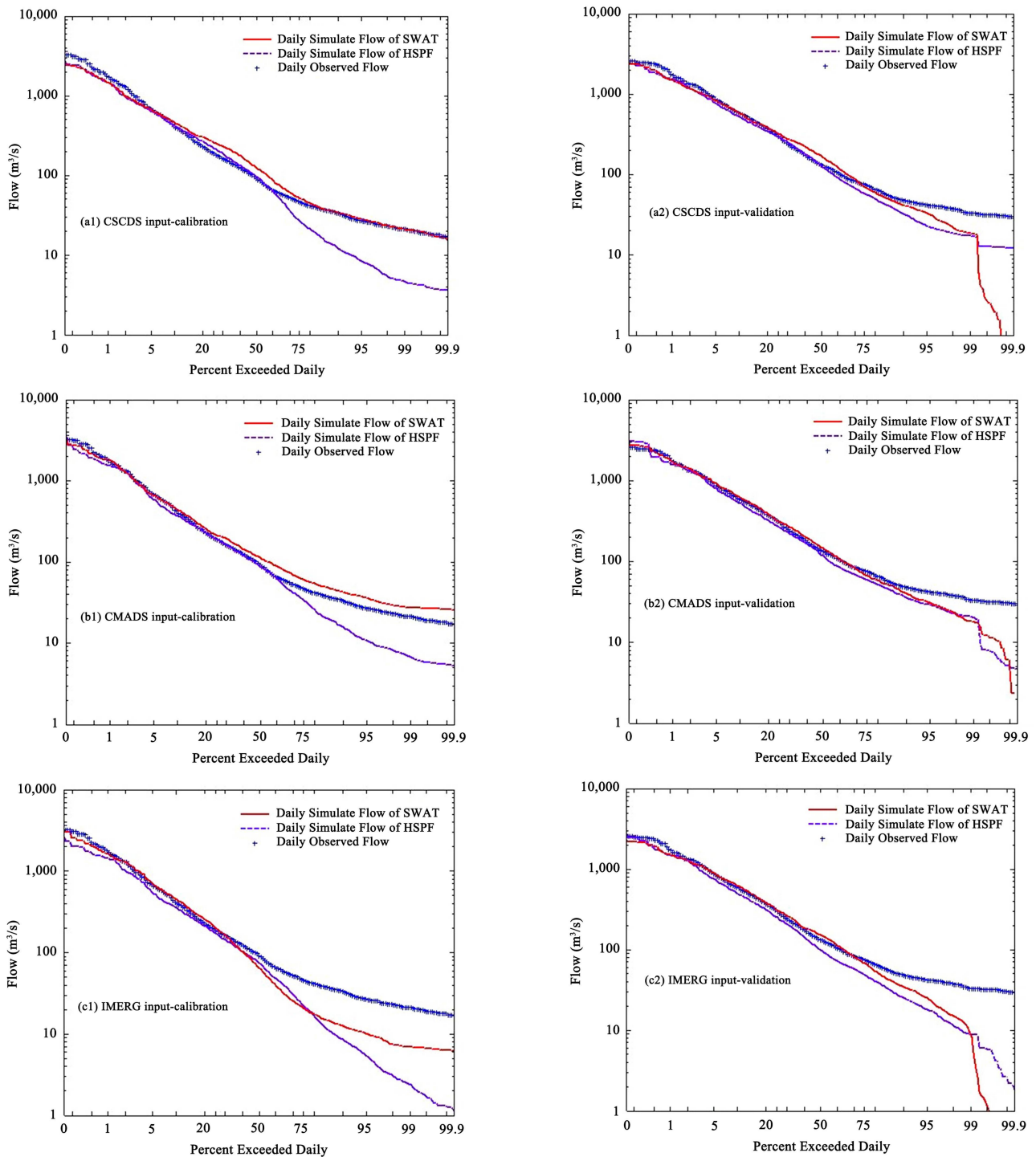

Figure 3. Comparison of the percentage of days when the SWAT and HSPF model results exceeded a certain flow with (**a1**,**a2**) CSCDS, (**b1**,**b2**) CMADS, and (**c1**,**c2**) IMERG inputs.

Table 4. Comparison of the simulation results of two models driven by three types of precipitation data.

Model	Precipitation Input	Calibration				Validation			
		NSE	R^2	RSR	MAE	NSE	R^2	RSR	MAE
SWAT	CMADS	0.78	0.78	0.49	64.30	0.76	0.78	0.52	79.33
	CSCDS	0.73	0.74	0.55	70.38	0.75	0.76	0.54	80.10
	IMERG	0.66	0.66	0.62	87.41	0.67	0.67	0.63	98.00
HSPF	CMADS	0.75	0.76	0.53	72.68	0.76	0.77	0.50	79.98
	CSCDS	0.73	0.74	0.55	77.46	0.74	0.76	0.54	82.67
	IMERG	0.66	0.66	0.62	80.24	0.71	0.73	0.59	82.35

3.2. Pollution Loading Simulation

According to the previous analysis results, the SWAT and HSPF models, when driven by CMADS precipitation data, produced the most accurate runoff simulation results in the Lijiang River Basin. Therefore, we chose to continue water quality simulations based on CMADS-data-driven hydrological simulations. Based on the runoff simulation results, we used the SWAT and HSPF models for monthly sediment simulation, and the simulation results are shown in Figure 4 with the statistical analysis provided in Table 5.

For the sediment simulation, the NSE and R^2 for the SWAT model simulations were all above 0.7, both in the calibration and the validation periods. The NSE and R^2 for the HSPF model simulations were above 0.6. The index value of simulation showed that both the SWAT and HSPF models produced ideal results. Compared to the HSPF simulation results, the SWAT model had a higher NSE and R^2, smaller RSR, and a similar MAE. In general, the SWAT model is better than the HSPF model for sediment simulation.

Ammonia nitrogen (NH_3-N) is a nutrient found in water bodies. Too high an ammonia nitrogen concentration will lead to eutrophication of the water body. Its decomposition and transformation consume oxygen in water, and it is toxic to aquatic animals and plants. Overall, the SWAT model more accurately simulated NH_3-N than the HSPF model. In addition, the average concentration of NH_3-N was simulated as 0.16 mg/L, which is in line with the national class II water quality standard in China (0.15–0.5 mg/L).

The amount of DO in water is an index used to measure the self-purification ability of a water body. We used the SWAT and HSPF models to simulate DO, and the simulation results are shown in Figure 4. The results showed that the simulations of the two models for sediment, NH_3-N, and DO were ideal and met the simulation requirements. Overall, the simulation effect produced by the SWAT model was more accurate than that of the HSPF model.

Through the comparative analysis of the water quality simulation effect of the two models and the evaluation of various water quality factors, we found that the water quality in the Lijiang River Basin can be categorized as class II water quality, and that the SWAT model is more suitable for water quality simulation. This laid the foundation for analyzing the sensitivity and uncertainty of the model parameters and provides a basis for the decision making regarding what agricultural management measures to implement.

3.3. Water Balance Analysis for Karst vs. Non-Karst Areas

We statistically analyzed the water balance of both karst and non-karst areas and the results are shown in Table S1, which shows that the average annual precipitation of the whole basin was approximately 1767.78 mm. The average annual precipitation in the karst and non-karst areas was approximately 1718.27 and 1817.29 mm, respectively. The precipitation trends in the two areas are similar, and the distribution of precipitation in the Lijiang River Basin was relatively uniform. The average annual evapotranspiration of the two areas was 530.56 and 532.20 mm, respectively, indicating that the evapotranspiration of the whole basin was relatively uniform. For surface runoff, the average annual surface runoff was approximately 677.33 mm in the karst areas and 749.61 mm in non-karst areas. The surface runoff in non-karst areas was larger than in karst areas, and this phenomenon was not only reflected in the average of many years, but also in the surface runoff in

non-karst areas being larger than in the karst areas for almost every year. The minimum difference in the surface runoff between the areas was approximately 17.77 mm, and the maximum difference was 204.29 mm. The reason for this difference is mainly the different geological landforms. The non-karst areas are dominated by clastic rock, the karst development is not obvious, the precipitation is mostly discharged in the form of surface runoff, and the recharge to groundwater is less than that in karst areas. The karst areas are mainly composed of hydrochloride rock with many pores and fissures, and the surface water can be quickly converted into groundwater. Our study of groundwater recharge confirms this finding. The average annual groundwater recharge was 492.72 mm in the karst areas and 358.46 mm in non-karst areas. The groundwater in the karst areas is active, and the amount of groundwater supplied by the surface every year is more than in the non-karst areas.
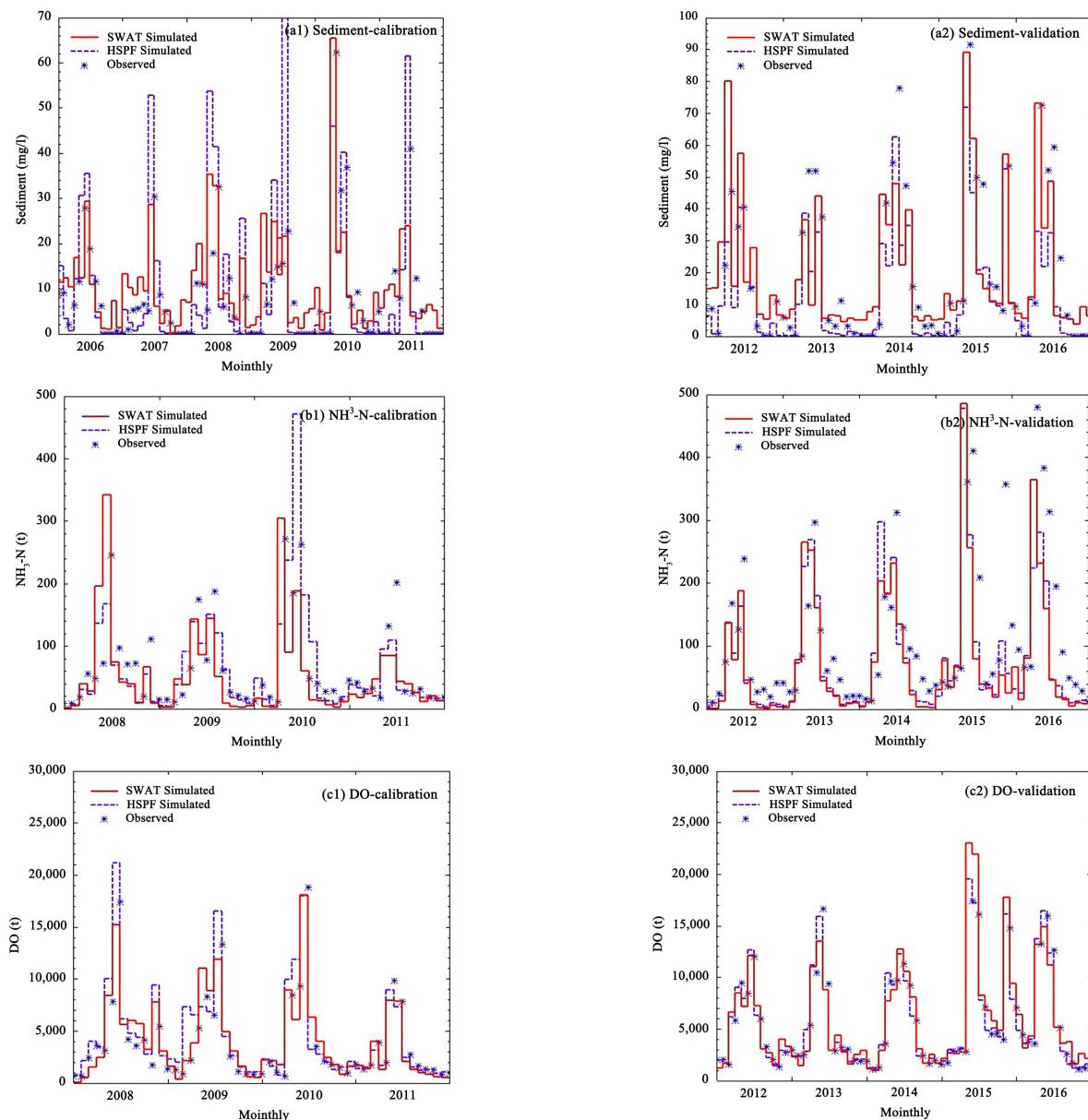

Figure 4. Comparison of the simulation results of two models: (**a1**,**a2**) sediment; (**b1**,**b2**) NH$_3$-N; (**c1**,**c2**) DO (calibration period: left; verification period: right).

Table 5. Summary of the water quality simulation indices used to evaluate the SWAT and HSPF models.

Parameters	Model	Calibration				Validation			
		NSE	R^2	RSR	MAE	NSE	R^2	RSR	MAE
Sediment	SWAT	0.74	0.75	0.60	3.74	0.62	0.70	0.59	8.86
	HSPF	0.70	0.70	1.03	5.32	0.61	0.70	0.60	8.25
NH$_3$-N	SWAT	0.63	0.71	0.63	32.73	0.60	0.70	0.55	47.19
	HSPF	0.61	0.66	0.75	37.26	0.60	0.68	0.57	48.40
DO	SWAT	0.85	0.90	0.39	1210.50	0.88	0.91	0.33	1066.30
	HSPF	0.73	0.81	0.39	1382.00	0.80	0.83	0.34	1150.82

Figures 5 and 6 show the water balance distribution of each sub-basin and the percentage that each water balance term contributed to the total precipitation for the karst and non-karst areas. The two figures display some differences between the water balance in karst and non-karst areas. The proportion of surface runoff and lateral flow in the non-karst areas was 46.00%, but only 41.42% in the karst areas, which shows that more runoff is generated in the former than in the latter. In addition, the percentages of groundwater recharge in non-karst and karst areas were 24.53% and 28.21%, respectively, and more water in the latter was used to recharge the groundwater. The ratio of karst and non-karst areas in this study area is close to 1:1, so the reason for this finding is mainly the difference of the geographical characteristics.
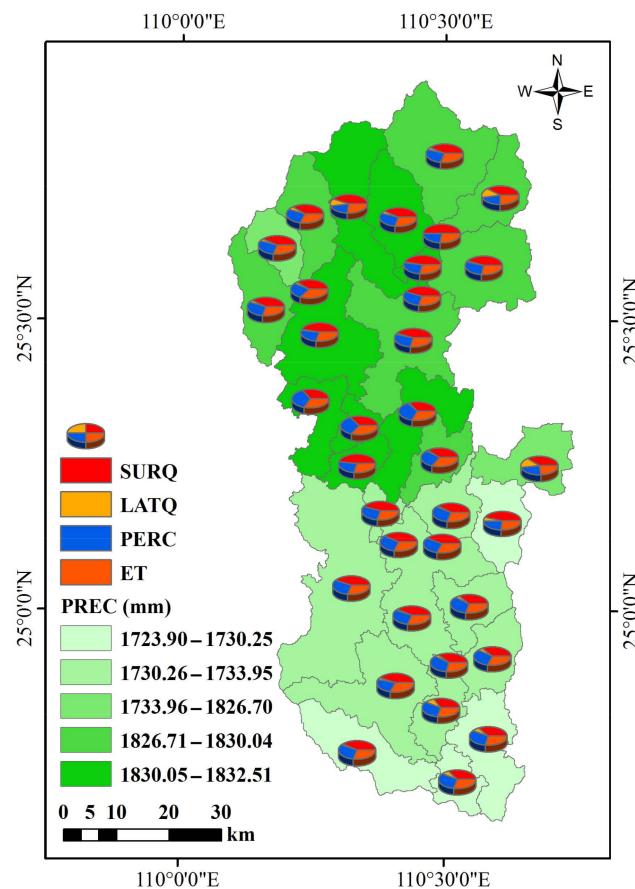

Figure 5. Water balance distribution map of the sub-basins (mm). SURQ is the surface runoff in the basin; LATQ is the lateral runoff; PERC is the recharge of soil to groundwater; and ET is the actual evapotranspiration.
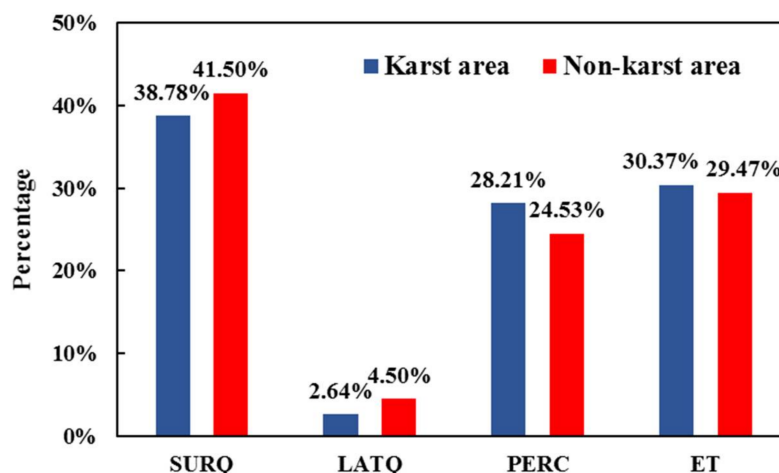
Figure 6. Percentage each water balance term contributed to total precipitation in karst and non-karst areas.

3.4. Pollution Load Analysis for Karst vs. Non-Karst Areas

Based on the water quality results output by the SWAT model, i.e., the sediment, we statistically analyzed the NH_3-N and DO pollution load per unit area in the karst and non-karst areas in the basin (Table 6). Figure 7 shows the distribution of pollution load per unit area in each sub-basin. For sediment, the sediment yield per unit area in the Lijiang River Basin was approximately 25.02 t/km^2, and the total sediment transport was approximately 13.62×10^4 t. The sediment yield per unit area was approximately 30.36 and 19.68 t/km^2 in the karst and non-karst areas, respectively. For NH_3-N, the load per unit area in the karst and non-karst areas was approximately 0.10^2 and 0.039 t/km^2, respectively; the total NH_3-N load in the karst and non-karst areas was approximately 281.01 and 104.87 t, respectively. The DO load per unit area in the karst and non-karst areas was approximately 4.930 and 4.203 t/km^2, respectively; the total DO load was approximately 1.36×10^4 and 1.13×10^4 t, respectively.

Table 6. Statistical table of unit pollution load in karst and non-karst areas (unit: t/km^2).

| Year	Sediment		NH_3-N		DO	
	Karst	Non-Karst	Karst	Non-Karst	Karst	Non-Karst
2006	25.2	14.05	0.098	0.032	5.023	4.463
2007	14.64	9.89	0.066	0.024	3.812	3.299
2008	26.81	22.51	0.117	0.048	5.126	4.498
2009	20.49	9.46	0.07	0.024	4.409	3.166
2010	16.09	14.27	0.079	0.035	4.632	3.715
2011	7.36	4.73	0.043	0.015	2.759	2.196
2012	34.59	30.64	0.145	0.061	4.996	4.196
2013	32.79	19.88	0.12	0.044	4.928	4.315
2014	35.49	18.58	0.107	0.041	5.171	4.479
2015	59.54	33.4	0.153	0.057	7.578	6.599
2016	60.94	39.02	0.122	0.054	5.796	5.312
Average	30.36	19.68	0.102	0.039	4.93	4.203
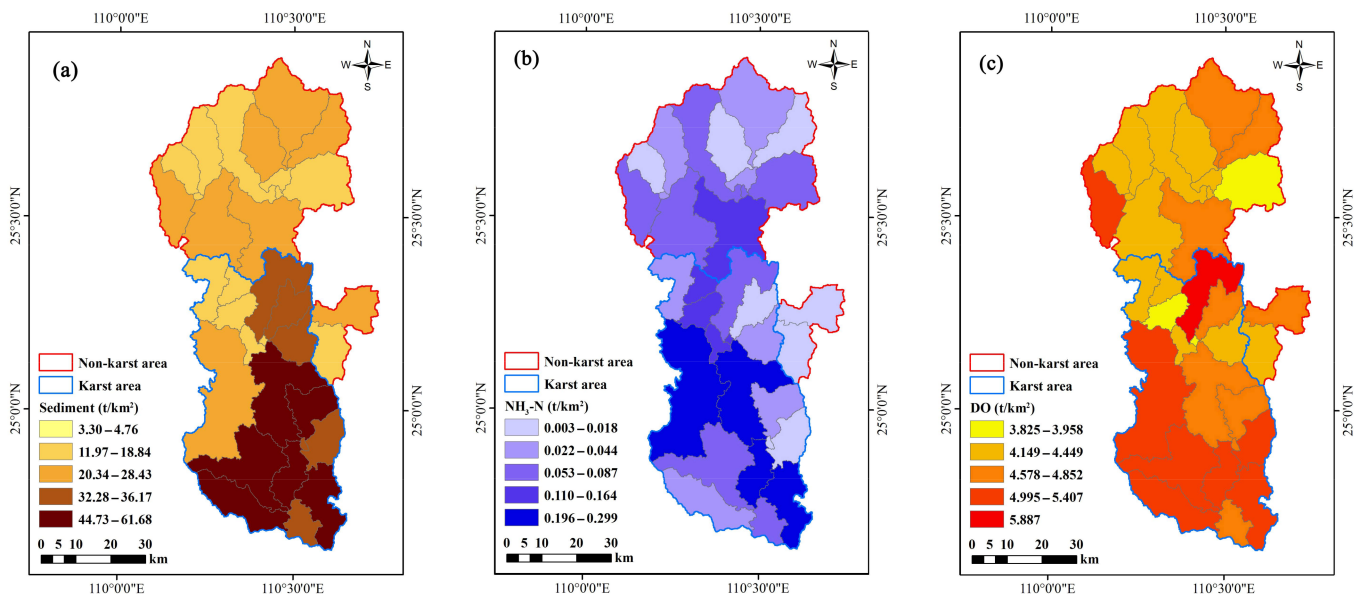
Figure 7. Spatial distribution of unit pollution load in each sub-basin (t/km^2): (**a**) sediment; (**b**) NH3-N; and (**c**) DO.

Figure 8 shows that the annual average sediment yield, NH$_3$-N, and DO pollution load in the karst areas were higher than in the non-karst areas. On the one hand, compared to clastic rock, carbonate rock is soluble, therefore the karst areas have a double-layer hydrogeological structure. This kind of geological structure leads to soil and water loss in a karst area through not only surface runoff with sediment carried by rainfall, but also by the leakage of soil particles into underground runoff through karst fissures and underground pipelines with rainfall. Similarly, the double circulation mechanism of the surface and the underground, pollutes both of them in a karst area at the same time, thereby increasing the amount of pollution. On the other hand, the area of cultivated land in the karst areas is approximately 1361 km^2, and that in the non-karst area is approximately 606 km^2. Therefore, there is more non-point-source pollution in the karst areas, leading to a higher pollution load of NH$_3$-N and DO.
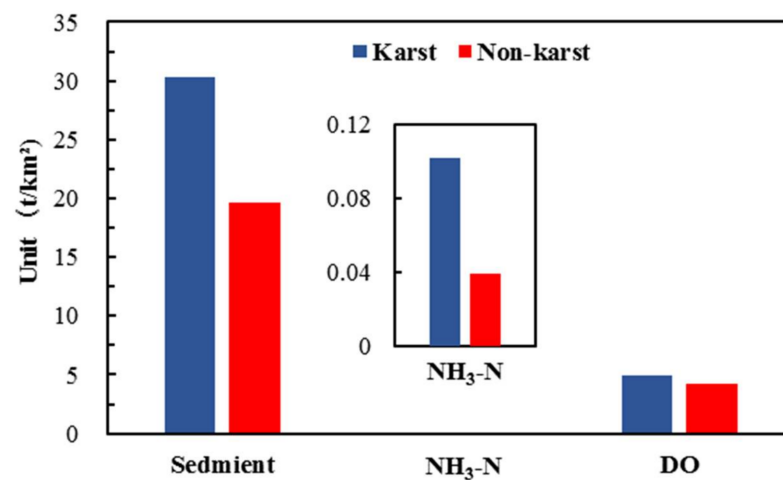

Figure 8. Diagram of the difference in annual average pollution load between the karst and non-karst areas.

3.5. Effect Evaluation of BMPs Reduction

3.5.1. Identification of Key Source Areas of Pollutants

The water quality in the Lijiang River Basin is relatively high, and the water quality assessments of the water source areas shows that the quality met the national standard; however, the overall water quality of the tributaries is lower than that of the main streams, and some of them have excessive pollution loads [41]. Due to the special geological and geomorphic forms of the karst areas, as well as the domestic sewage, animal husbandry, farmland fertilization, and so on, in the area, the problems of soil erosion and agricultural non-point-source pollution still exist in the Lijiang River Basin. Using the SWAT model to simulate and evaluate management measures is an effective method to prevent and control non-point-source pollution.

To ensure management measures are accurate and effective, the locations and sources of pollutants must be identified first, that is, the key sources of pollutants must be identified. The study area mainly includes four areas: Xing'an County, Lingchuan County, Guilin City, and Yangshuo County. The fertilization of farmland in the four counties and cities is planned after consulting the data [42]. The pollutants we studied were NH_3-N and DO, and the main types of fertilizer applied in the area are nitrogen, phosphorus, and compound fertilizer (N:P:K = 1:1:1). We converted the amount of fertilizer according to the proportion of cultivated land area in each sub-basin to the planting area of the four counties and cities. Figure 9a,b depicts the distribution map of cultivated land area and the fertilization amount in each sub-basin, respectively. Combined with the area of cultivated land, the amount of applied fertilizer, and the distribution of unit pollutant load, we identified the key source areas of pollutants as six sub-basins: 26, 29, 31, 32, 34, and 35. Table 7 lists the cultivated land area, fertilization amount, and pollutant load in these six sub-basins.
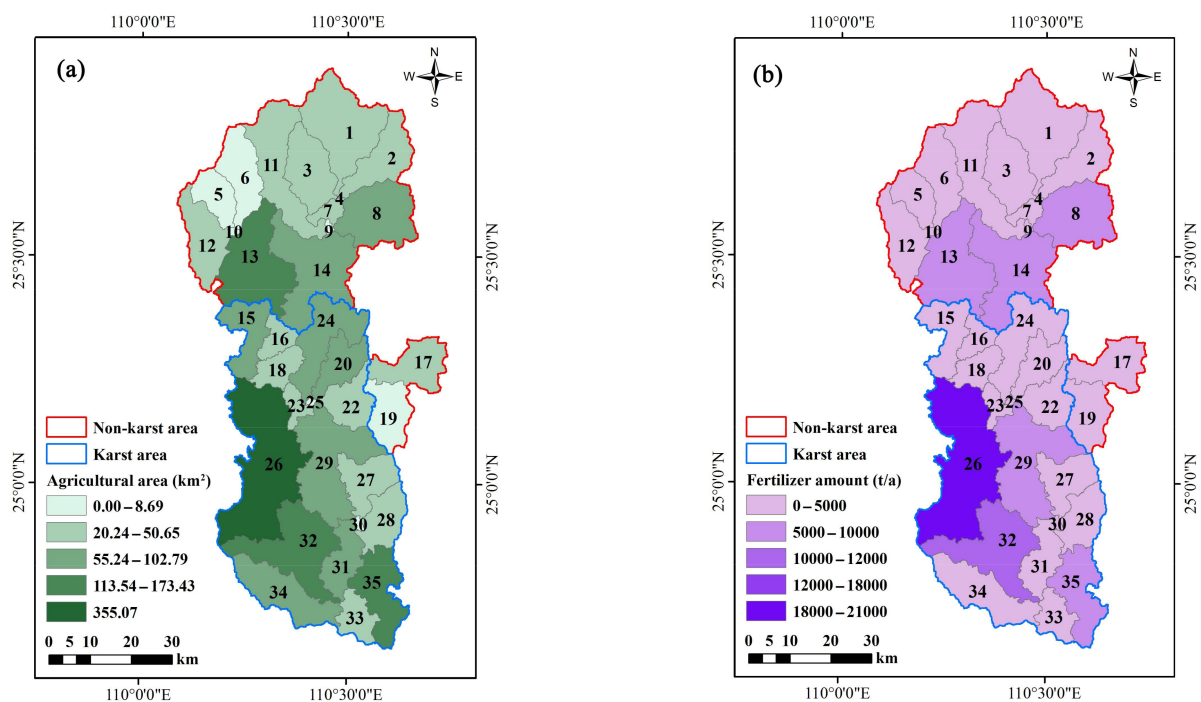

Figure 9. Maps of the distribution of (**a**) cultivated land (km^2) and (**b**) fertilization (t/a) in each sub-basin.

Table 7. Statistical table of cultivated land area, fertilization amount, and pollutant load amount in key source areas.

Sub-Basin Number	Cultivated Land Area (km^2)	Fertilization (t/a)	Sediment (t/km^2)	NH$_3$-N (t/km^2)	DO (t/km^2)
26	355.07	20,458.36	23.31	0.299	5.304
29	95.57	5506.68	49.93	0.196	4.711
31	59.42	3423.84	50.34	0.224	5.407
32	173.07	9972.17	47.38	0.059	4.995
34	80.72	4650.72	45.7	0.043	5.071
35	113.54	6541.98	44.73	0.239	5.336

3.5.2. Evaluation of the Effect of BMPs on Pollution Reduction

In this study, we evaluated the effects of seven scenarios on the reduction in NH$_3$-N and DO pollution loads at the sub-basin scale. The results are shown in Table 8 and Figure 10. In general, the efficiency of BMPs in reducing NH$_3$-N load, in descending order was: returning farmland to forest > vegetation buffer zone > contour hedgerow > grassed waterway > stubble mulching > no tillage. The efficiency of DO load reduction, in descending order was: vegetation buffer zone > grass channel > returning farmland to forest > equal height hedgerow > stubble cover > no tillage.

Table 8. The rates of NH$_3$-N and DO reductions by implementing BMPs in different scenarios.

BMPs Scenario	NH$_3$-N (t/km^2)			DO (t/km^2)		
	Load	Reduction	Reduction Rate	Load	Reduction	Reduction Rate
0 (Initial)	0.081	—	—	4.567	—	—
1 (No tillage)	0.075	0.006	7.41%	4.514	0.053	1.16%
2 (Stubble mulching)	0.069	0.012	14.81%	4.503	0.064	1.40%
3 (Vegetation buffer zone)	0.058	0.023	28.40%	4.377	0.19	4.16%
4 (Grassed waterway)	0.063	0.019	23.46%	4.401	0.166	3.63%
5 (Contour hedgerow)	0.061	0.02	24.69%	4.490	0.077	1.69%
6 (Returning farmland to forest)	0.053	0.028	34.57%	4.425	0.142	3.11%
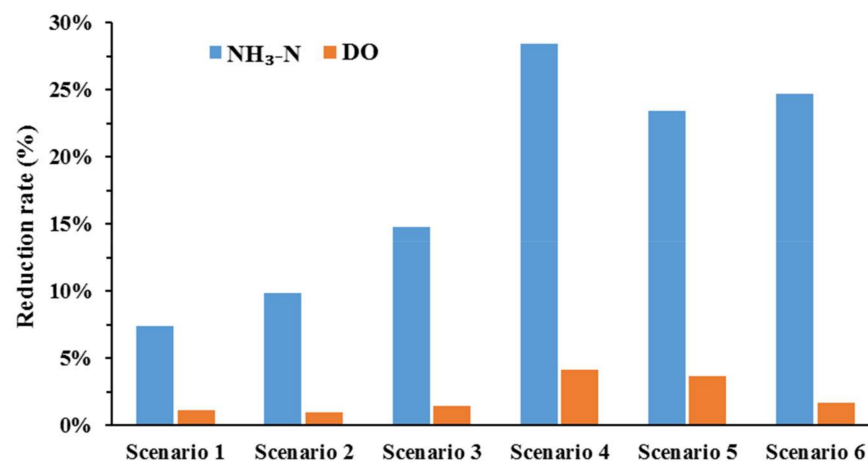
Figure 10. Reduction rate of NH$_3$-N and DO load by implementing BMPs in different scenarios.

In scenario 1, NH$_3$-N and DO loads were reduced 7.41% and 1.16%, respectively; in scenario 2, the loads were reduced 14.81% and 1.40%, respectively. Stubble mulching was more effective than no-till measures in reducing pollution loads, and both practices were more effective in reducing NH$_3$-N than DO. The reduction efficiency of NH$_3$-N and DO

loads in scenario 3 was 28.40% and 4.16%, respectively, and 23.46% and 3.63%, respectively, in scenario 4, demonstrating the increased reduction effect of these two measures. It may be because planting aquatic plants can intercept pollution on the one hand, and, on the other hand, the process of aquatic plant growth and respiration can absorb nitrogen and consume dissolved oxygen to reduce the eutrophication of water bodies. The reduction efficiency of scenario 5 on NH_3-N and DO loads was 24.69% and 1.69%, respectively. This measure mainly indirectly controls pollution loads by reducing soil erosion, so the reduction effect is slightly inferior to that of vegetated buffer strips and grassed waterways. Scenario 6 can directly reduce the arable land area and effectively control the surface source pollution, and the reduction efficiency of NH_3-N and DO loads was 34.57% and 3.11%, respectively. Its pollution load reduction rate is effective, especially for the NH_3-N load.

In summary, the six scenarios reduced the NH_3-N and DO pollution load, and the reduction in NH_3-N was more obvious than that of DO; however, the reduction rate is low, with a maximum of 34.57%. For NH_3-N, the main reason is that nitrogen-containing pollutants include organic nitrogen, ammonia nitrogen, nitrate nitrogen, nitrite nitrogen, etc., and ammonia nitrogen only accounts for a part of the total. The proportion of ammonia nitrogen in chemical fertilizer is low, therefore, although the amount of farmland fertilization in the basin is large, the total amount of ammonia nitrogen pollutants is low, resulting in a low reduction rate. For DO, water bodies have a strong self-purification ability; aquatic animals and plants can quickly consume excess DO, so that the DO reaches a balanced state without the implementation of external measures. Planting trees and grass can speed up the process.

4. Conclusions

In this study, we first evaluated the performance of three meteorological data-driven SWAT and HSPF models for runoff and water quality simulations in the Lijiang River Basin. The simulation results showed that the combination of the three meteorological data and the two models can meet the requirements for simulating runoff in the Lijiang River Basin, but the simulation results differed due to the differences in meteorological data resolution and values. Amongst the considered data, the CMADS data performed the best, the CMADS-driven SWAT model was able to achieve an NSE and R^2 above 0.75, and the errors represented by RSR and MAE were the smallest, indicating that this combination is the most suitable amongst the considered combinations. In addition, sediment, NH_3-N, and DO were simulated well for the Lijiang River Basin. The CMADS data can be used for similar areas where ground-based observation sites are sparse or missing.

Because of the special geological formation of the Lijiang River Basin, we divided the basin into karst and non-karst areas to analyze more targeted water resource management measures. Due to the karst areas having more pores and fissures, the recharge of groundwater by precipitation is greater in these areas than that in non-karst areas. The surface runoff in non-karst areas is higher than that in karst areas; the sediment yield, NH_3-N, and DO loads per unit area in karst areas are higher than in non-karst areas. Therefore, the need for the prevention and control of non-point-source pollution in karst areas is greater.

Finally, we set up six BMPs scenarios in the extracted critical pollution source areas to evaluate the effects of different management measures on reducing NH_3-N and DO loads. Among them, the reduction effects of two measures, returning farmland to forest and a vegetation buffer zone, were the most obvious, with the highest reduction efficiency of 34.57% and 4.16% being achieved for NH_3-N and DO, respectively. There are various types of agricultural surface pollutants, but due to our insufficient information on water quality, only two types of pollutants were selected in this study. Representative pollutants such as total nitrogen and total phosphorus will be selected as control objects when available, and more accurate management measures will be developed based on this study.

References

1. Li, Y. The evolution of implication of karst and its environmental protection. *Carsol. Sin.* **2009**, *19*, 260–267.
2. Bai, J. Karst Tourism Resources and Their Characteristics in Guangxi. Master's Thesis, Guangxi Normal University, Guilin, China, 2010.
3. Zhou, Y.; Chen, Q.; Sun, K.; Chen, S.; Xu, X.; Wang, J.; Chai, M.; Zhang, J. Distribution characteristics and development model of karst in Hunan area. *J. China Univ. Petroleum. Ed. Natrual Sci.* **2020**, *44*, 163–173.
4. Worthington, S.R.H. Diagnostic hydrogeologic characteristics of a karst aquifer (Kentucky, USA). *Hydrogeol. J.* **2009**, *17*, 1665–1678. [CrossRef]
5. Doummar, J.; Sauter, M.; Geyer, T. Simulation of flow processes in a large scale karst system with an integrated catchment model (Mike She)—Identification of relevant parameters influencing spring discharge. *J. Hydrol.* **2012**, *426–427*, 112–123. [CrossRef]
6. Zhu, B.; Yang, Q.; Yunqiu, X.; Yan, D.; Tang, M.; Liu, D.; Zeng, H. Spatial distribution and driving factors of karst rocky desertification in Lijiang River basin. *J. Guangxi Norm. Univ. Nat. Sci. Ed.* **2021**, *39*, 139–150. [CrossRef]
7. Aouissi, J.; Benabdallah, S.; Chabaâne, Z.L.; Cudennec, C. Sensitivity analysis of SWAT model to the spatial rainfall distribution and watershed subdivision in streamflow simulations in the Mediterranean context: A case study in the Joumine watershed. Tunisia. In Proceedings of the 2013 5th International Conference on Modeling, Simulation and Applied Optimization (ICMSAO), Hammamet, Tunisia, 28–30 April 2013; pp. 1–6.
8. Boufala, M.H.; El Hmaidi, A.; Chadli, K.; Essahlaoui, A.; El Ouali, A.; Taia, S. Hydrological modeling of water and soil resources in the basin upstream of the Allal El Fassi dam (Upper Sebou watershed, Morocco). *Model. Earth Syst. Environ.* **2019**, *5*, 1163–1177. [CrossRef]
9. Wang, J.; Zhang, X.-H.; Xu, C.-Y.; Wang, H.; Lei, X.-H.; Wang, X.; Li, S.-Y. Development of load duration curve system in data-scarce watersheds based on a distributed hydrological model. *Hydrol. Res.* **2019**, *50*, 886–900. [CrossRef]
10. Rudra, R.P.; Mekonnen, B.A.; Shukla, R.; Shrestha, N.K.; Goel, P.K.; Daggupati, P.; Biswas, A. Currents Status, Challenges, and Future Directions in Identifying Critical Source Areas for Non-Point Source Pollution in Canadian Conditions. *Agriculture* **2020**, *10*, 468. [CrossRef]
11. Arnold, J.G.; Fohrer, N. SWAT2000: Current capabilities and research opportunities in applied watershed modelling. *Hydrol. Processes* **2005**, *19*, 563–572. [CrossRef]
12. Zhou, F.; Xu, Y.; Chen, Y.; Xu, C.Y.; Gao, Y.; Du, J. Hydrological response to urbanization at different spatio-temporal scales simulated by coupling of CLUE-S and the SWAT model in the Yangtze River Delta region. *J. Hydrol.* **2013**, *485*, 113–125. [CrossRef]
13. Xu, H.; Xu, C.-Y.; Sælthun, N.R.; Xu, Y.; Zhou, B.; Chen, H. Entropy theory based multi-criteria resampling of rain gauge networks for hydrological modelling—A case study of humid area in southern China. *J. Hydrol.* **2015**, *525*, 138–151. [CrossRef]
14. Wang, X.; Liang, Z.; Wang, J. Simulation of Runoff in Karst-influenced Lianjiang Watershed Using the SWAT Model. *Sci. J. Earth Sci.* **2014**, *4*, 85–92.
15. Tian, Y.; Wang, S.; Bai, X.; Luo, G.; Xu, Y. Trade-offs among ecosystem services in a typical Karst watershed, SW China. *Sci. Total Environ.* **2016**, *566–567*, 1297–1308. [CrossRef]
16. Lin, Z. Estimating Water Budgets and Vertical Leakages for Karst Lakes in North-Central Florida (United States) Via Hydrological Modeling1. *JAWRA J. Am. Water Resour. Assoc.* **2011**, *47*, 287–302. [CrossRef]
17. Buchanan, C.; Moltz, H.L.N.; Haywood, H.C.; Palmer, J.B.; Griggs, A.N. A test of The Ecological Limits of Hydrologic Alteration (ELOHA) method for determining environmental flows in the Potomac River basin, USA. *Freshw. Biol.* **2013**, *58*, 2632–2647. [CrossRef]
18. Ren, P.; Li, J.; Feng, P.; Guo, Y.; Ma, Q. Evaluation of Multiple Satellite Precipitation Products and Their Use in Hydrological Modelling over the Luanhe River Basin, China. *Water* **2018**, *10*, 677. [CrossRef]

19. Jiang, L.; Bauer-Gottwein, P. How do GPM IMERG precipitation estimates perform as hydrological model forcing? Evaluation for 300 catchments across Mainland China. *J. Hydrol.* **2019**, *572*, 486–500. [CrossRef]

20. Zhao, P.; Li, B.; Wang, J.; Yang, H.; Guo, P.; Gong, L. Accuracy Evaluation and Comparison of GPM IMERG and ERA5 Precipitation Products over Complex Terrain of Yunnan. *Meteorol. Sci. Technol.* **2021**, *49*, 114–123. [CrossRef]

21. Meng, X.Y.; Wang, H.; Lei, X.H.; Cai, S.Y.; Wu, H.J.; Ji, X.N.; Wang, J.H. Hydrological modeling in the Manas River Basin using soil and water assessment tool driven by CMADS. *Teh. Vjesn.* **2017**, *24*, 525–534. [CrossRef]

22. Meng, X.; Wang, H.; Wu, Y.; Long, A.; Wang, J.; Shi, C.; Ji, X. Investigating spatiotemporal changes of the land-surface processes in Xinjiang using high-resolution CLM3.5 and CLDAS: Soil temperature. *Sci. Rep.* **2017**, *7*, 13286. [CrossRef]

23. Wu, Y.; Chen, J. Analyzing the Water Budget and Hydrological Characteristics and Responses to Land Use in a Monsoonal Climate River Basin in South China. *Environ. Manag.* **2013**, *51*, 1174–1186. [CrossRef]

24. Guo, B.; Zhang, J.; Xu, T.; Croke, B.; Jakeman, A.; Song, Y.; Yang, Q.; Lei, X.; Liao, W. Applicability Assessment and Uncertainty Analysis of Multi-Precipitation Datasets for the Simulation of Hydrologic Models. *Water* **2018**, *10*, 1611. [CrossRef]

25. Smith, E.A.; Asrar, G.; Furuhama, Y.; Ginati, A.; Mugnai, A.; Nakamura, K.; Adler, R.F.; Chou, M.-D.; Desbois, M.; Durning, J.F.; et al. International Global Precipitation Measurement (GPM) Program and Mission: An Overview. In *Measuring Precipitation From Space: EURAINSAT and the Future*; Levizzani, V., Bauer, P., Turk, F.J., Eds.; Springer: Dordrecht, The Netherlands, 2007; pp. 611–653.

26. Meneghini, R.; Iguchi, T.; Kozu, T.; Liao, L.; Okamoto, K.; Jones, J.A.; Kwiatkowski, J. Use of the surface reference technique for path attenuation estimates from the TRMM precipitation radar. *J. Appl. Meteorol.* **2000**, *39*, 2053–2070. [CrossRef]

27. Su, J.B.; Li, X.; Ren, W.W.; Lu, H.S.; Zheng, D.H. How reliable are the satellite-based precipitation estimations in guiding hydrological modelling in South China? *J. Hydrol.* **2021**, *602*, 17. [CrossRef]

28. Boufala, M.; El Hmaidi, A.; Essahlaoui, A.; Chadli, K.; El Ouali, A.; Lahjouj, A. Assessment of the best management practices under a semi-arid basin using SWAT model (case of M'dez watershed, Morocco). *Model. Earth Syst. Environ.* **2021**, 1–9. [CrossRef]

29. Sun, Q.; Zhang, C.; Yu, X.; Li, J.; Zhang, Y.; Gao, Y. Best management practices of agricultural non-point source pollution in China: A review. *Chin. J. Ecol.* **2013**, *32*, 772–778. [CrossRef]

30. Arabi, M.; Govindaraju, R.S.; Hantush, M.M.; Engel, B.A. Role of Watershed Subdivision on Modeling the Effectiveness of Best Management Practices With SWAT. *J. Am. Water Resour.* **2006**, *42*, 513–528. [CrossRef]

31. Okumah, M.; Martin-Ortega, J.; Chapman, P.J.; Novo, P.; Cassidy, R.; Lyon, C.; Higgins, A.; Doody, D. The role of experiential learning in the adoption of best land management practices. *Land Use Pol.* **2021**, *105*, 12. [CrossRef]

32. Huang, Z.; Chen, Y.; Jiang, Y.; Cheng, Y. Analysis on Water Resources of Lijiang River Basin. *J. Guangxi Acad. Sci.* **2005**, *21*, 56–60.

33. Cai, D.; Ma, Z. Main Ecological Problems in Lijiang River Watershed. *J. Guangxi Norm. Univ. Nat. Sci. Ed.* **2008**, *26*, 110–112.

34. Zhao, H.; Xiao, Q.; Wu, X.; Liu, F.; Miao, Y.; Jiang, Y. Impact of Human Activities on Water-Rock Interactions in Surface Water of Lijiang River. *Environ. Sci.* **2017**, *38*, 4108–4119. [CrossRef]

35. Liang, G. Study on Water Resources Assessment Based on SWAT Model-A Case Study of Liji. Master's Thesis, China University of Geosciences (Beijing), Beijing, China, 2019.

36. Jing, Y. Applications of water-balance principle to analysis and calculation for water-consumption of river basin. *Northwest Water Resour. Water Eng.* **2003**, *2*, 30–32.

37. Moriasi, D.N.; Arnold, J.G.; Van Liew, M.W.; Bingner, R.L.; Harmel, R.D.; Veith, T.L. Model evaluation guidelines for systematic quantification of accuracy in watershed simulations. *Trans. ASABE* **2007**, *50*, 885–900. [CrossRef]

38. Ahmad, H.M.N.; Sinclair, A.; Jamieson, R.; Madani, A.; Hebb, D.; Havard, P.; Yiridoe, E.K. Modeling Sediment and Nitrogen Export from a Rural Watershed in Eastern Canada Using the Soil and Water Assessment Tool. *J. Environ. Qual.* **2011**, *40*, 1182–1194. [CrossRef] [PubMed]

39. Ghoraba, S.M. Hydrological modeling of the Simly Dam watershed (Pakistan) using GIS and SWAT model. *Alex. Eng. J.* **2015**, *54*, 583–594. [CrossRef]

40. Huang, K. Research on Non-Point Source Pollution Management Measures of Danjiang River Basin Based on SWAT Model. Master's, Thesis, Xi'an University of Technology, Xi'an, China, 2020.

41. Zhang, Z. Water Environment Assessment and Analysis of Pollution Sources in the Upper Reaches of Lijiang River Basin. Master's, Thesis, Guilin University of Technology, Guilin, China, 2021.

42. Liu, X.; Li, S. Investigation of Rural and Agricultural Pollution Source in Lijiang River Basin in Guilin. *Hubei Agric. Sci.* **2015**, *54*, 3372–3375. [CrossRef]